

FRACTURE AND CRACK PROPAGATION OF METALLIC BILAYERS USING QUASI-CONTINUUM SIMULATIONS

C. D. WU^a, T. H. FANG^{b,*}, W. C. SU^b, Y. C. FAN^b

^a*Department of Mechanical Engineering, Chung Yuan Christian University, Taoyuan 32023, Taiwan*

^b*Department of Mechanical Engineering, National Kaohsiung University of Science and Technology, Kaohsiung 80778, Taiwan*

The effects of the constituting material, initial crack length, and crystal orientation on the fracture and mechanics of bilayers with an interface crack under tension are studied using quasi-continuum simulations in terms of atomic trajectories, strain distribution, the stress-strain curve, and the crack growth-strain curve. The simulation results show that at the initial tension stage, the bilayers exhibit linear elasticity regardless of initial crack length and constituting material. With an increase in initial crack length at a layer interface, the yield stress, yield strain, and ultimate stress of the bilayers decrease. Bilayers with longer initial crack under tension have faster crack growth. Bilayers with a structural orientation of [020] versus $[10\bar{1}]$ have lower mechanical strength compared to that of those with structural orientations of [100] versus [010] and $[\bar{1}10]$ versus [010]. The Ni/Ni bilayer has the highest yield stress and ultimate stress under tension.

(Received November 11, 2019; Accepted April 7, 2020)

Keywords: Bilayer, Quasi-continuum method, Stress, Strain, Dislocation

1. Introduction

Nanoscale metallic multilayers have received a lot of attention due to their superior mechanical properties and other physical properties, such as high hardness [1], good fatigue strength [2], excellent wear resistance [3], strong magnetism [4], and high thermal stability [5]. Dislocation propagation in these multilayers is greatly suppressed by the interfaces between layers, leading to high mechanical strength. The relationship between mechanical strength and individual layer thickness can be described by the Hall-Petch scaling law.

A nanoscale crack may be introduced in multilayers during manufacturing or normal use, especially at the layer interface, creating a weakness for multilayers. Therefore, detailed information on the deformation and fracture of multilayers is essential for the safe use of these

* Corresponding author: fang.tehua@msa.hinet.net

materials. However, obtaining such information through experimental observations is very challenging and expensive. Molecular dynamics (MD) simulation is a common tool for studying nanoscale materials and mechanics. Yuan et al. [6] modeled a Cu/Ag bilayer under biaxial tension using MD simulation. They found that dislocations are prone to nucleate at the layer interface and propagate toward the free surfaces. The Cu/Ag bilayer had higher yield strain than those of pure Cu and Ag films. Breaking occurs at the layer interface when the temperature or tensile velocity is increased [7]. Wang et al. [8] simulated the influence of interface shear strength on the interaction of lattice glide dislocations with face-centered cubic/body-centered cubic interfaces. They found that the nucleation and gliding of interfacial dislocations are dominated by the atomic structures of the interfaces regardless of the interface shear strength. Wu and Jian [9] modeled Au/Cu multilayers under indentation and found that layer interfaces act as strong barriers that resist the propagation of dislocations, even at an extremely small individual layer thickness of 3 nm.

Although MD simulation is very useful for studying nano system, the simulation of localized deformation requires the use of relatively large systems, which may result in error accumulation if MD is used directly. The quasi-continuum (QC) method [10-12] uses local and non-local atom regions for seamless bridging between the atomic and continuum regions. The purpose of the present work is to study the effects of the constituting material, initial crack length, and crystal orientation of metallic bilayers on fracture and mechanics via QC simulation. The results are discussed in terms of atomic trajectories, strain distribution, the stress-strain curve, and the crack growth-strain curve.

2. Model and methodology

Fig. 1(a) shows a schematic illustration of the Ni/Ni bilayer fracture simulation. Tension is applied to the top of a bilayer that contains an interface crack until fracture. Fig. 1(b) shows the QC model. An interface nano crack is created by removing the atoms at the upper and lower crack surfaces. Three types of bilayer, namely Ni/Ni, Cu/Ni, and Cu/Cu, are used to investigate the effect of the constituting material. The dimensions of the bilayers are 20 nm (X) \times 30 nm (Y). The initial crack width (W) is set to 1.76 nm and the initial crack length (L) is varied in the ranges of 4.4 - 8.5 nm to investigate the effect of the initial crack length. The crystal orientation of the bilayer is X [100], Y [010], and Z [001]. A periodic boundary condition is applied in the X- and Z-directions of the model for approximating a large system.

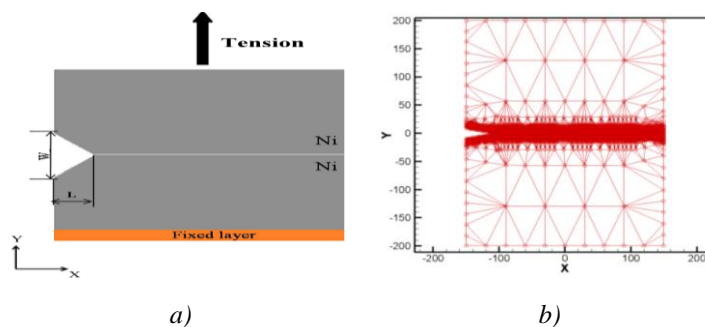


Fig. 1. (a) Schematic illustration of Ni/Ni bilayer fracture simulation and (b) corresponding QC model. Many non-local atoms are set around the bilayer interface to accurately capture the fracture process.

Two types of atom, local and non-local atoms, are set in the model. The local atoms are used for uniform deformation areas, such as areas far away from the layer interface. The energies of these atoms are calculated based on the Cauchy-Born rule [13]. Non-local atoms are set around the layer interface to accurately capture localized deformation, as shown in Fig. 1(b). The embedded-atom method [14] is adopted to describe the interaction of the non-local atoms of Ni-Ni, Ni-Cu, and Cu-Cu, respectively. The top- and bottom-most layers are set as boundary and rigid layers, respectively. A constant displacement of 0.2 nm per step along the Y-direction is applied to the boundary layer until fracture. The boundary layer is used to apply tension to the whole system while the rigid layer is used to support it.

3. Results and discussion

Figs. 2(a) - (c) show the variation of strain versus tensile stress for the Ni/Ni, Cu/Cu, and Ni/Cu bilayers for L values of 4.4, 6.5, and 8.5 Å, respectively. At the initial stage of tensile deformation, the tensile stress rapidly and linearly increases with increasing strain, indicating an elastic deformation stage for each bilayer, regardless of initial crack length and constituting material. The slope of the stress curve decreases with increasing initial crack length, which is in good agreement with a previous report [15]. For L values of 4.4 and 6.5 Å, the magnitude of the slope of the stress curves follows the order: Ni/Ni > Cu/Cu > Ni/Cu; however, the slope of Ni/Cu becomes slightly higher than that of Cu/Cu when the L value increases to 8.5 Å. The Ni/Ni bilayer has the highest Young's modulus; those of Cu/Cu and Ni/Cu are similar. The linear part of the stress curves for Ni/Ni, Cu/Cu, and Ni/Cu bilayers end sat a peak stress point, namely the yield stress, which increases with increasing strain rate and decreasing temperature [16]. The yield stress for Ni/Ni, Cu/Cu, and Ni/Cu is 8.0, 5.0, and 4.9 G Pa for $L= 4.4$ Å, 7.1, 4.0, and 4.2 G Pa for $L=6.5$ Å, and 4.9, 3.3, and 3.2 G Pa for $L= 6.5$ Å, respectively. The Ni/Ni bilayer exhibits the highest yield stress; those of Cu/Cu and Ni/Cu are similar. The relationship between yield strain, the constituting material, and L value is unclear. The stress curves then drop with increasing strain and exhibit significant oscillation due to the formation of nucleation sites and the propagation of dislocations from the interface to release tensile stress. The relationship between the stress curve

oscillation mode, constituting material, and L value also seems unclear. The Ni/Ni bilayer has the highest ultimate stress; those of Cu/Cu and Ni/Cu are similar. The yield stress, yield strain, and ultimate stress decrease with increasing L value, which indicates that bilayers with a larger L value have lower mechanical strength and fracture earlier. This also shows good consistency with the previous studies [17-19].

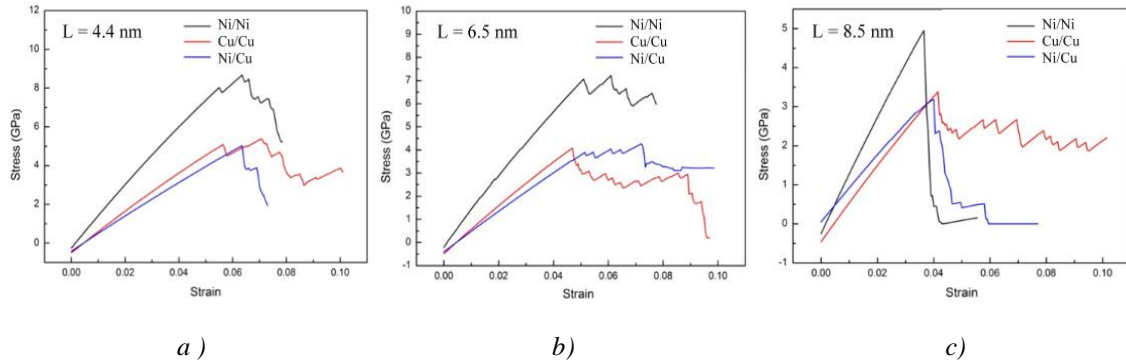


Fig. 2. Variation of strain versus tensile stress for Ni/Ni, Cu/Cu, and Ni/Cu bilayers for L values of (a) 4.4, (b) 6.5, and (c) 8.5 Å.

Fig. 3(a)-(c) show snapshots of the Ni/Ni, Cu/Cu, Ni/Cu bilayers, respectively, during the tensile test at strains of 0.025, 0.050, and 0.075, with an L value of 0.65 Å. The atoms are color-coded according to the magnitude of their equivalent strain values. Atoms with relatively high equivalent strain values mainly appear around the crack tip due to high-speed crack growth under tension. A significant dislocation first nucleates at the Cu/Cu interface and propagates along the close-packed direction [110] toward the upper Cu layer at a strain of 0.050; for the Ni/Ni and Ni/Cu bilayers, similar dislocations nucleate and propagate at a higher strain (0.075). The number of dislocations increases with increasing strain, indicating plastic crack growth for the bilayers. The equivalent strain values of the atoms around the crack tip dramatically increase once dislocations format the interface, which indicates that the dislocation formation promotes crack growth.

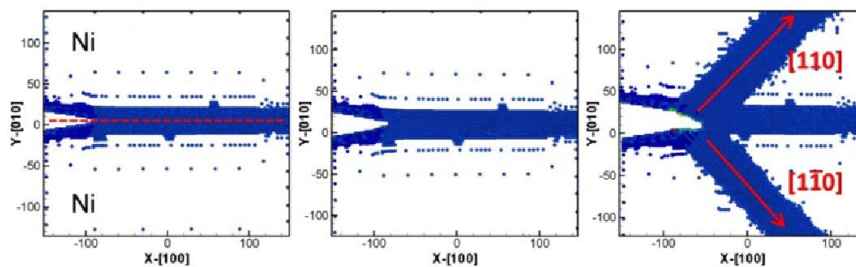


Fig. 3a). Snapshots of Ni/Ni bilayers during tensile test at strains of 0.025, 0.050, and 0.075, with and L value of 0.65 Å. Atoms are color-coded according to the magnitude of their equivalent strain values.

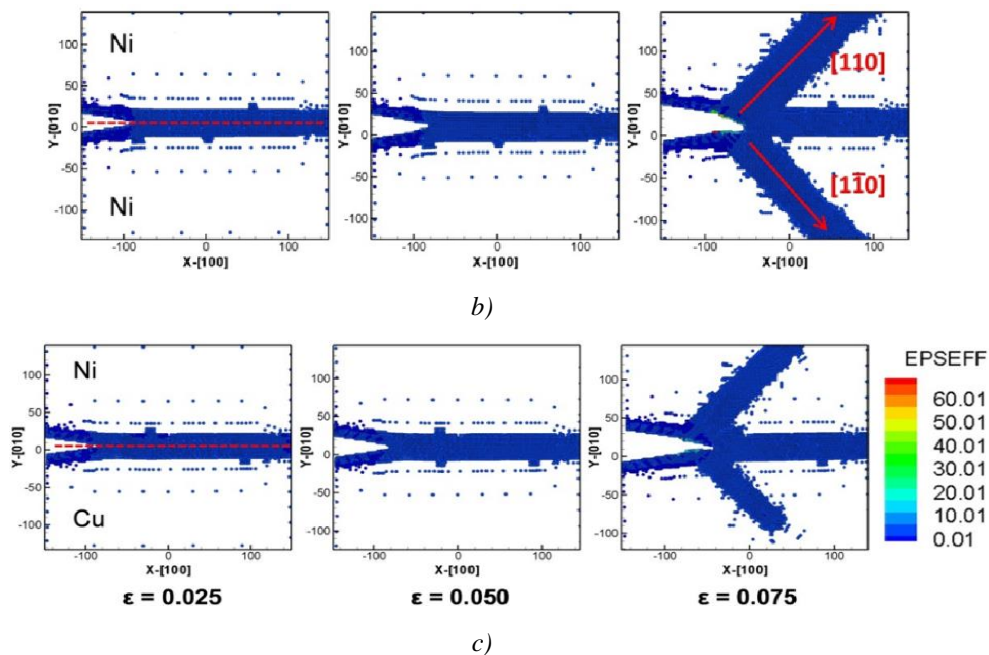


Fig. 3. Snapshots of (b) Cu/Cu, and (c) Ni/Cu bilayers during tensile test at strains of 0.025, 0.050, and 0.075, with and L value of 0.65 \AA . Atoms are color-coded according to the magnitude of their equivalent strain values.

Fig. 4 shows the variation of strain versus crack growth for the Ni/Ni, Cu/Cu, and Ni/Cu bilayers for an L value of 6.5 \AA . The relationship between strain and crack growth is completely nonlinear and difficult to predict. At the initial crack growth stage (strain < 0.050), Cu/Cu is relatively sensitive to strain; for example, the crack length for Cu/Cu increases to 30 \AA when the strain increases to 0.048 , whereas that for Ni/Ni and Ni/Cu is less than 10 \AA at the same strain. The crack growth for Cu/Cu then slightly slows down with increasing strain, and that for Ni/Cu and Ni/Ni gradually speeds up. Overall, Cu/Cu and Ni/Cu have the highest and lowest crack growth speeds, respectively.

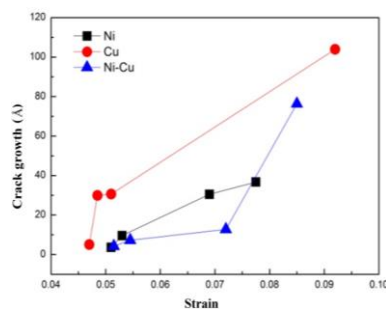


Fig. 4 Variation of strain versus crack growth for Ni/Ni, Cu/Cu, and Ni/Cu bilayers for an L value of 6.5 \AA .

Figs. 5(a)-(c) show snapshots of the Ni/Cu bilayer during the tensile test at various strain values for L values of 4.4, 6.5, and 8.5 Å, respectively. For larger L values, crack growth becomes faster with an increase in strain. To study the effect of the structural orientation of the bilayers, structural orientations of [100] versus [010] (mode I), $[\bar{1}10]$ versus [010] (mode II), and [020] versus $[10\bar{1}]$ (mode III), respectively, corresponding to the X and Y directions of the bilayers, respectively, are tested. Fig. 6 shows the variation of strain versus tensile stress for the Ni/Cu bilayer during the tensile test for an L value of 6.5 Å for the three structural orientations. The trends of the stress-strain curves for structural orientation modes I and II are very similar, whereas the stress significantly drops for structural orientation mode III. The structural orientation effects on the stress-strain curves for the Ni/Ni and Cu/Cu bilayers are also the same. This indicates that bilayers with structural orientation modes I and II are more resistant to local shear deformation, and that with orientation mode III has lower mechanical strength.

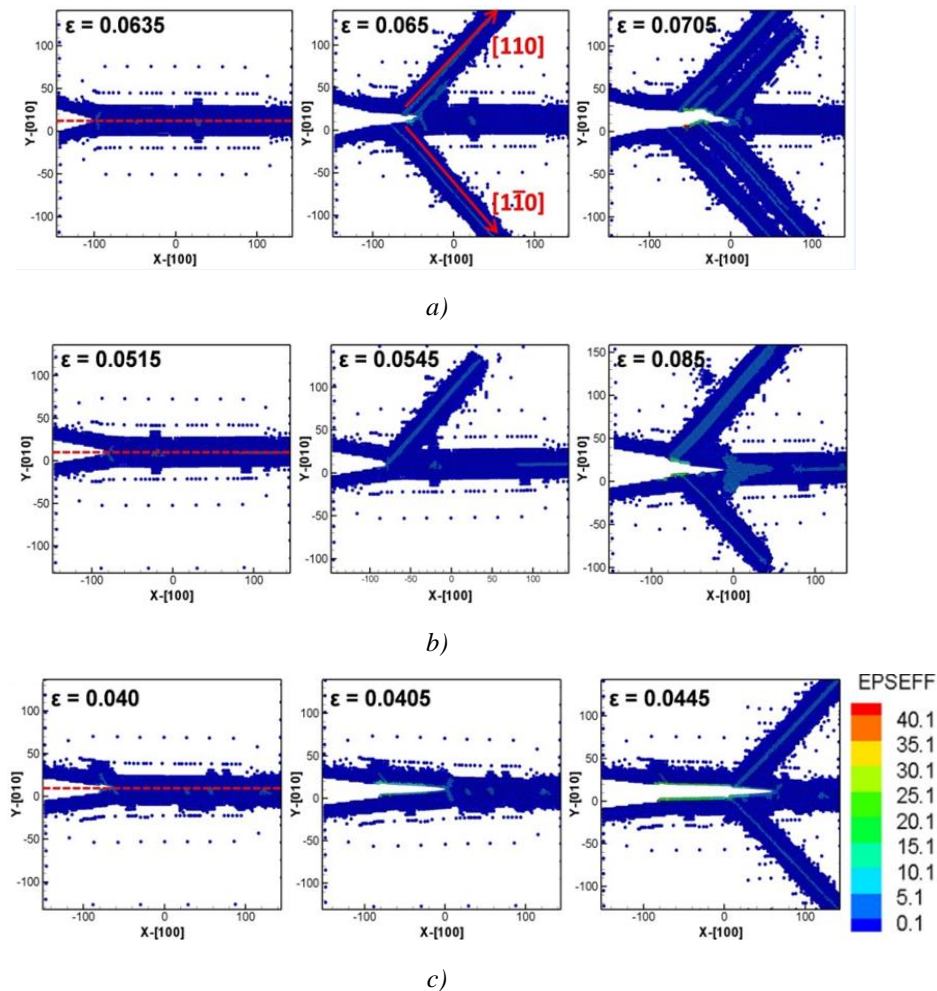


Fig. 5. Snapshots of Ni/Cu bilayer during tensile test at various strain values for L values of (a) 4.4, (b) 6.5, and (c) 8.5 Å.

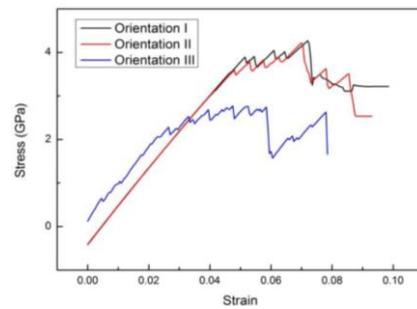


Fig. 6. Variation of strain versus tensile stress of Ni/Cu bilayer during tensile test for an L value of 6.5 \AA for three structural orientations.

Figs. 7(a)-(c) show snapshots of the Ni/Cu bilayer during the tensile test at strain values of 0.025, 0.050, and 0.075 for an L value of 6.5 \AA for the three structural orientations, respectively. Comparing structural orientation modes I and II, shown in Figs. 7(a) and (b), the bilayer with structural orientation mode II forms dislocations first, at a strain of 0.050, resulting in an earlier termination of elastic deformation (see Fig. 6, red line). The bilayer with structural orientation mode III has a more complicated fracture pattern, including the formation of dislocations along the $[111]$ direction and a twin deformation at a strain of 0.075.

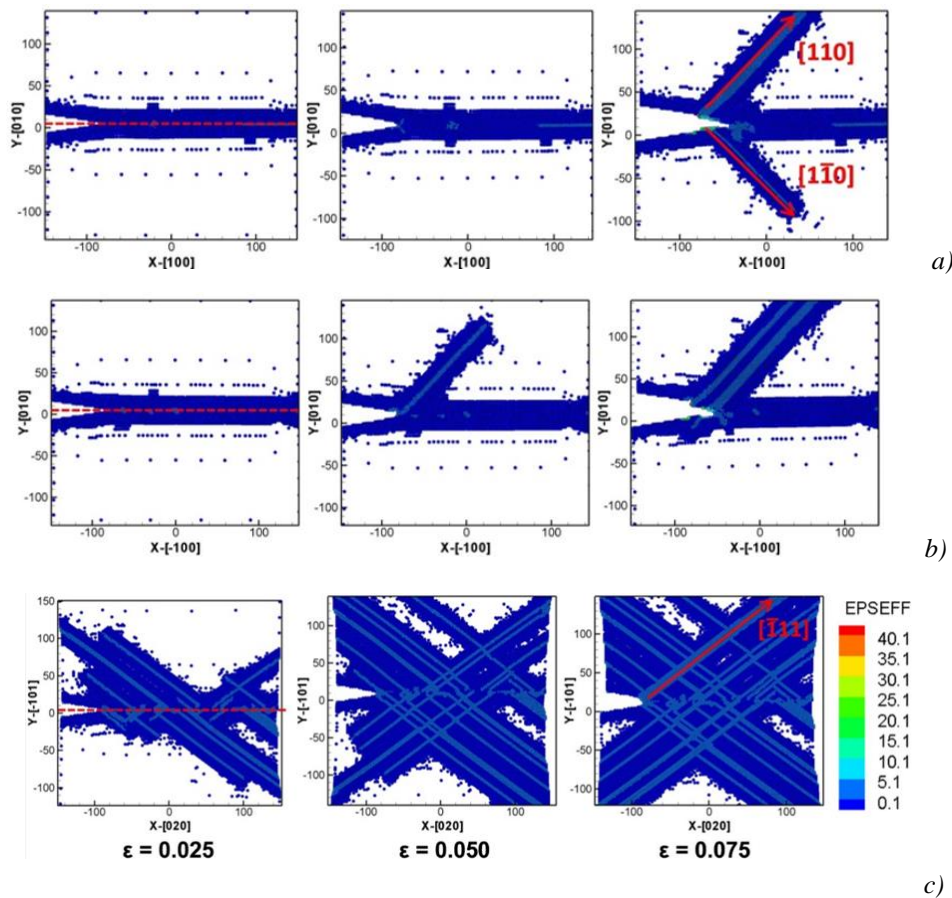


Fig. 7. Snapshots of Ni/Cu bilayer during tensile test at strain values of 0.025, 0.050, and 0.075 for an L value of 6.5 \AA for structural orientations of (a) $[100]$ versus $[010]$, (b) $[\bar{1}10]$ versus $[010]$, and (c) $[020]$ versus $[10\bar{1}]$.

4. Conclusion

This work investigated the effects of the constituting material, initial crack length, and crystal orientation of bilayers on fracture and mechanics using QC simulation. The following conclusions were obtained:

The elastic deformation of the bilayers ends once a dislocation forms at the layer interface. This dislocation results in an increase in crack growth. The yield stress, yield strain, and ultimate stress decrease with increasing initial crack length.

The Ni/Ni bilayer has the highest yield stress and ultimate stress. Bilayers with a longer initial crack have faster crack growth.

Bilayers with a structural orientation of [020] versus $[10\bar{1}]$ have lower mechanical strength compared to that of those with structural orientations of [100] versus [010] and $[\bar{1}10]$ versus [010].

Acknowledgments

The authors acknowledge the support by the Ministry of Science and Technology, Taiwan under grant numbers MOST106-2221-E-992-333-MY3 and MOST106-2221-E-992-343-MY3.

References

- [1] A. Misra, M. Verdier, Y. C. Lu, H. Kung, T. E. Mitchell, M. Nastasi, J. D. Embury, *Scripta Materialia* **39**, 555 (1998).
- [2] X. F. Zhu, G. P. Zhang, *Journal of Physics D: Applied Physics* **42**, 055411 (2009).
- [3] S. P. Wen, R. L. Zong, F. Zeng, Y. Gao, F. Pan, *Wear* **265**, 1808 (2008).
- [4] X. Li, B. Bhushan, *Thin Solid Films* **398-399**, 313 (2001).
- [5] S. Zheng, I. J. Beyerlein, J. S. Carpenter, K. Kang, J. Wang, W. Han, N. A. Mara, *Nature Communications* **4**, 1696 (2013).
- [6] L. Yuan, Z. Xu, D. Shan, B. Guo. *Applied Surface Science* **282**, 450 (2013).
- [7] C. D. Wu, W. X. Jiang, *Thin Solid Films* **638**, 258 (2017).
- [8] J. Wang, R. G. Hoagland, X. Y. Liu, A. Misra, *Acta Materialia* **59** (8), 3164 (2011).
- [9] C. D. Wu, W. X. Jiang, *Journal of Molecular Modeling* **24**(9), 253 (2018).
- [10] R. E. Miller, E. B. Tadmor, *Journal of Computer-Aided Materials Design* **9**, 203 (2002).
- [11] C. D. Wu, T. H. Fang, Y. J. Lin, *Journal of molecular modeling* **24**(9), 222 (2018)
- [12] A. S. Tran, T. H. Fang, L. R. Tsai, C. H. Chen, *Journal of Physics and Chemistry of Solids* **126**, 180 (2019)
- [13] V. B. Shenoy, R. Miller, E. B. Tadmor, D. Rodney, R. Phillips, M. Ortiz, *Journal of the Mechanics and Physics of Solids* **47**, 611 (1999).

- [14] J. S. Amelang, G. N. Venturini, D. M. Kochmann, *Journal of the Mechanics and Physics of Solids* **82**, 378 (2015).
- [15] C. B. Cui, H. G. Beom, *Computational Materials Science* **118**, 133 (2016).
- [16] B. Zhang, L. Zhou, Y. Sun, W. He, Y. Chen, *Molecular Simulation* **44** (15), 1252 (2018).
- [17] R. Z. Qiu, Y. C. Lin, T. H. Fang, L. R. Tsai, *Materials Research Express* **4**(3), 035019 (2017).
- [18] R. Z. Qiu, Y. C. Lin, T. H. Fang, *Beilstein Journal of Nanotechnology* **9**(1), 1000 (2018).
- [19] T. H. Fang, W. J. Chang, P. C. Cheng, *Digest Journal of Nanomaterials and Biostructures* **11**(1), 23 (2016).